Transplantation of human umbilical cord mesenchymal stem cells induces angiogenesis and promotes repair of uterine scars in rats

xiuyin shen (SXY1204@126.com)
Maternity and Children Hospital https://orcid.org/0000-0002-6753-6251

Xin Luo
Maternity and Children Hospital

Shuzhen Wu
Maternity and Children Hospital

Yingchun Wan
Maternity and Children Hospital

Huiting Ma
Maternity and Children Hospital

Shaoxin Ye
Maternity and Children Hospital

Zhuoling Zhang
Maternity and Children Hospital

Min Lu
Maternity and Children Hospital

Hai Tang
Maternity and Children Hospital

Xiaoyan Gou
Maternity and Children Hospital

Xiaoling Guo
Maternity and Children Hospital

Zhengping Liu
Maternity and Children Hospital https://orcid.org/0000-0002-4964-0258

Research Article

Keywords: hUC-MSC transplantation, uterine scars, angiogenesis, repairment

Posted Date: August 22nd, 2022

DOI: https://doi.org/10.21203/rs.3.rs-1871903/v1

Abstract

Background

Uterine scar after cesarean section (CS) is an important cause of intrauterine adhesion, amenorrhea, uterine rupture, and infertility in females. Disruptions of angiogenesis play a critical role in the healing of uterine scars. In this study, we investigated the effects of human umbilical cord mesenchymal stem cells (hUC-MSCs) on angiogenesis regeneration in uterine scars in rats following full-thickness excision of uterine walls.

Methods

Approximately 2.0 cm was excised along the uterine wall in each uterine horn to establish a rat model of uterine scars. Hematoxylin and eosin (H&E) staining was applied to observe the tissue structure. Masson trichrome staining was used to reveal collagen deposition. Angiogenesis factors (FGF-2, VEGFA, and PDGFB) were detected via western blotting. The fate of transplanted hUC-MSCs was assessed using *in vivo* fluorescence imaging. The differential expression of microRNA and function prediction was detected using high-throughput sequencing.

Results

hUC-MSCs significantly improved the morphology of the tissue structure and alleviated fibrosis in general on days 15, 30, and 60 of transplantation in the hUC-MSC groups. Moreover, the expressions of all three angiogenesis factors were increased at days 15 and 30 post-transplantation. In GFP analyses, although hUC-MSCs were observed on the uterine wall at days 15 and 30, those signals gradually weakened and then accumulated in other organs at day 60. In addition, abundant hUC-MSC-specific microRNAs targeted the cell pathways of angiogenesis and the PI3K/AKT signaling pathway.

Conclusion

hUC-MSC transplantation contributed to the repair of uterine scars, mainly through the suppression of excessive fibrosis and the enhancement of vascular remodeling.

Introduction

Rates of cesarean section (CS) have been increasing worldwide in recent years. A study that included data from 169 countries covering 98.4% of the world's births indicated that the number of CS births in 2015 (29.7 million, 21.1%) were double the rate in 2000 (16.0 million, 12.1%) [1]. Although CS has become an effective treatment for maternal women [2, 3], it can lead to several complications, including postoperative thrombosis, intraoperative bleeding, uterine rupture, placenta previa, and cesarean scar

pregnancy (CSP) [4]. In a previous study, the incidence of CSP was 1:2226–1:1800 in 1.15% of women with previous CS deliveries [5]. Moreover, CSP can cause massive hemorrhage and uterine rupture, infertility, or even loss of life [6]. These serious adverse outcomes associated with uterine scars are a significant concern. Therefore, it is of great clinical importance to explore possible interventions to repair the injured uterus.

In the last few years, mesenchymal stromal cells (MSCs) have been used in a new therapy for wound healing [7–11]. Their use can play a critical role in treating burn wounds by promoting cell migration, proliferation, and differentiation, while suppressing immune reactions [12–14]. Moreover, MSCs can effectively accelerate cutaneous wound closure [15–19]. Recently, human umbilical cord MSCs (hUC-MSCs) have been widely used to repair injured tissue

because of their multiple sources and easy availability, low immunogenicity, strong proliferation ability, and other beneficial properties. They are an ideal choice for cell therapy. These cells promote the recovery of thin endometrium *in vivo* [20], differentiate into functional endothelial cells, and promote revascularization [21]. Women with intrauterine adhesion who receive hUC-MSC therapy show improved fertility outcomes with minimal side effects [22–24].

CS can lead to loss of resident stem cells and impair the basalis of the endometrium, which may trigger the continuous secretion of collagen and excessive activation of fibroblasts, leading to the formation of scars. hUC-MSCs facilitate collagen degradation in uterine scars in rats [25], and can impact CS skin scars [26, 27]. However, the exact mechanisms underlying any such effects remain incompletely elucidated. In this study, we investigated the effects of hUC-MSCs on revascularization in uterine scars in rats following the full-thickness excision of uterine walls.

Methods

hUC-MSC cultures

The hUC-MSCs used in this study were a generous gift from the Beijing Health & Biotech group (Beijing, China). The cells were incubated at 37°C in a humid atmosphere consisting of 5% CO_2 and then in a complete growth medium consisting of DMEM/F12 and GlutaMAX™ (Gibco,USA) supplemented with 10% fetal bovine serum (FBS; Thermo Fisher Scientific Life Sciences), 100 U/mL penicillin (Gibco,USA), and 100 μg/mL streptomycin (Gibco,USA). The cells were passaged when they reached 90% confluence. hUC-MSCs in passages 3–5 were used for the following experiments.

Cell-cycle analysis

hUC-MSCs were seeded in a six-well culture plate. When they reached 80% confluence, the cells were collected and washed with PBS. RNase A solution (100 μL) was added, and the cells were incubated for 30 min at 37°C. Finally, 400 μL PI was added and incubated for 30 min at room temperature. The DNA

content was detected by flow cytometry. The data were analyzed by CytExpert. The percentage of cells in the G1 phase, the S phase, the G2 phase, and the M phase was analyzed.

CCK8 assay

Cell counting kit-8 (CCK8) was used to evaluate the proliferation and viability of hUC-MSCs. The cells were seeded in 96-well plates at a concentration of 5×10^3 cells/well and were incubated with 10 μL CCK8 (5 mg/mL) (Dojindo) at 37°C for 4 h. The CCK8 assay was performed every 24 h for 7 days. The absorbance of each well was measured at a wavelength of 450 nm using a spectrophotometric plate reader.

Differentiation of hUC-MSC

The morphologies of hUC-MSCs were observed through an inverted microscope at P3, and representative pictures were captured at 10×. Moreover, adipogenic, osteogenic, and chondroblastic differentiation assays were used to verify the multi-lineage differentiation potential of the cells. Adipogenesis was induced by adipogenic induction medium (Gibco) for 14 days and was confirmed by Oil red O staining to show the intracellular lipid accumulation. Chondroblasts were induced using chondroblastic induction medium (Gibco) for 21 days and confirmed by alcian blue staining to show acidic mucopolysaccharide accumulation. Osteogenesis was induced using osteogenic induction medium (Gibco) for 21 days, and calcium deposition was shown by Alizarin red staining.

Flow cytometry analysis

hUC-MSC surface antigens were analyzed via flow cytometry. In brief, after reaching 80% confluency, adherent cells were harvested. In all, 1×10^6 cells were incubated with 1% bovine serum albumin (BSA)/PBS (Gibco) for 30 min to block nonspecific antigens. Subsequently, the cells were incubated with phycoerythrin (PE)-conjugated anti-rat CD34 (BD Pharmingen), CD73 (BD Pharmingen), and CD105 (BD Pharmingen), as well as fluorescein isothiocyanate (FITC)-labeled anti-rat CD45 (BD Pharmingen) and CD90 (BD Pharmingen) in the dark at 4°C for 30 min. The cells were washed twice with 1% BSA/PBS, resuspended in 200 μL 1% BSA/PBS, and analyzed using a flow cytometer (Beckman DxFLEX, USA).

Establishment of a rat model of uterine scars

Nine-week-old female Sprague-Dawley (SD) rats weighing between 200 g and 250 g (SPF level, Guangzhou University of Chinese Medicine, SCXK [Guangzhou] 2013–0034) were used. Four to five rats were housed per cage at room temperature (25±1°C), with ambient humidity (70±4%), light/dark cycle 12 h/12 h, and free access to food and water.

Twenty rats that were not pregnant were categorized into the ‘normal’ group. Then, 100 pregnant rats were randomly assigned to four groups. In the natural group, rats underwent natural labor without any treatment. The CS group did not undergo any treatment after CS. In the PBS group, 0.5 mL PBS was injected per uterine horn after CS. The hUC-MSC group had 5×10^6 hUC-MSCs injected per uterine horn

after CS. Under sterile surgical conditions, rats were anesthetized with intraperitoneal injection of 10% chloral hydrate (35 mg/kg). The abdominal wall was opened to expose the uterine horns, the Y-type uterus was slowly taken out and the fetuses were removed, the uterus was sutured, and then PBS and hUC-MSCs were injected (Fig. 1). All rats after CS received an intramuscular injection of penicillin twice a day for 3 days.

Hematoxylin and eosin (H&E) staining

H&E staining was applied to observe the tissue structure. The tissues were paraffin embedded using the usual processes, sliced (4 μm), and stained with H&E. A LEICA DMi1 inverted phase-contrast microscope was used to observe histomorphological changes in the rat uterus.

Masson trichrome staining

Masson trichrome staining was used to observe the collagen deposition. The tissues were paraffin embedded with regular processes, sliced (4 μm), and stained with Masson. A LEICA DMi1 inverted phase-contrast microscope was used to observe fibrosis in different groups.

Western blotting

The tissues were quickly removed and homogenized via sonication in RIPA buffer (Beyotime). The tissues were lysed at 4°C for 30 min and centrifuged at 12,000 rpm for 20 min. Protein concentrations were determined using the Pierce™ BCA Protein Assay Kit (Thermo Fisher Scientific, Inc.). Equal amounts of protein were subjected to standard western blotting. Subsequently, PVDF membranes (Millipore) were incubated overnight at 4°C with primary antibodies, anti-FGF2 (1:1000, A0235, Abclonal), anti-PDGFB (1:1000, ab178409, Abcam), anti-VEGFA (1:1000, ab214424, Abcam), and anti-GAPDH (1:1000, ab8245, Abcam). Then the membranes were incubated with secondary HRP-conjugated antibody (1:10,000) at room temperature for 1 h. Detection was performed using Super ECL Plus (Beyotime).

In vivo fluorescence imaging

hUC-MSCs were infected with GFP-expressing lentiviral vectors. Before cell transplantation, GFP expression in the hUC-MSCs was verified using a fluorescence microscope. Cells were trypsinized for 1 min, and the suspension was collected and centrifuged at 1300 rpm for 6 min. The final cell pellet was suspended in PBS at a final density of 5×10^6 cells/mL. Using a Hamilton syringe, 2.5×10^6 GFP-labeled hUC-MSCs in 100 μL PBS were evenly injected at three positions per uterine horn after CS along the incision. We used a planar fluorescence imaging station, Night OWL II LB983 (Berthold Technologies USA), to acquire fluorescent images.

High-throughput sequencing

The rats were sacrificed after anesthesia on day 60. The abdominal wall was opened to expose the uterine horns, and 1.0 cm samples of scar, uniform in diameter, were removed from the uterine incision.

Scar specimens were preserved in liquid nitrogen. Sequencing was performed by Aksomics Biotechnology Co. The targeted mRNA of hUC-MSC-specific microRNAs were predicted using miRDB (available at http://mirdb.org/). The functions and pathway analyses of these mRNA targets were predicted using DAVID (available at https://david.ncifcrf.gov/).

Statistical analysis

Statistical analysis was performed using Prism 7.0 c software (GraphPad, San Diego, USA). Quantitative data were extracted as means ± standard deviations from at least three independent experiments. Paired-group comparisons were performed using a t-test and multiple-group comparisons were determined with one-way analysis of variance. Values of $P < 0.05$ were considered statistically significant.

Results

hUC-MSC culture and identification

hUC-MSCs maintained a mesenchymal-like morphology (Fig. 2A). We detected the distribution of the cell cycle via flow cytometry to analyze the cellular DNA content. As shown in Fig. 2B, the percentage of HMC cells was 45.61% in the G0/G1 phase and 54.39% in the S + G2 + M phases. Moreover, the proliferation ability of the cells was measured using a growth curve (Fig. 2C). The cells showed the potential for osteogenic differentiation, chondroblastic differentiation, and adipogenic differentiation (Fig. 2D–F). The immunophenotyping of hUC-MSCs at P4 was analyzed by flow cytometry, and the results showed that CD73 (96.57), CD90 (99.64), and CD105 (98.58) were positive indicators, while CD34 (0.12) and CD45 (0.07) were negative ones (Fig. 2J, K).

hUC-MSCs ameliorate the morphological features of the uterus

The macroscopic appearance of the uterus was examined at days 15, 30, and 60 after CS. At day 15, excrescences in uterine scars were more apparent in the PBS and CS groups than in hUC-MSCs. At day 30, these excrescences became more obvious and contractures also appeared. At day 60, those two groups showed severe tissue edema. In contrast, in the hUC-MSCs group, the macroscopic appearance of the uterus was similar to those of the normal and natural groups (Fig. 3A). To better evaluate the repair of uterine scars, we performed H&E staining. The basic structures of the uterine scars in the CS and PBS groups were disorganized at days 15, 30, and 60 after CS, while the glands and blood vessels were clearly visible in the hUC-MSC group at days 15, 30, and 60 (Fig. 3B). According to Masson’s trichrome staining results, the scars in the CS and PBS groups showed abundant collagen deposition at days 15, 30, and 60. Nevertheless, the hUC-MSCs group showed obvious muscle bundles and collagen degradation (Fig. 3C).

hUC-MSC transplantation facilitates angiogenesis in uterine scars via upregulation of angiogenesis-related factors

FGF-2, VEGFA, and PDGFB play critical roles in angiogenesis. Their expression in uterine scars reflects the angiogenesis potential of hUC-MSCs. To examine the effects of hUC-MSCs on uterine scar healing, we evaluated their levels. As shown in Fig. 4, compared to the CS group, FGF-2, VEGFA, and PDGFB levels were greatly increased in the hUC-MSCs group at days 15 and 30. To accurately assess the therapeutic effects of hUC-MSCs, we further calculated their levels at day 60. There were no significant differences among the PBS, CS, and hUC-MSCs groups. The expressions of all factors were significantly lower in these groups than in the normal and natural labor groups. This is presumably because hUC-MSCs migrate to other organs, which is consistent with the *in vivo* fluorescence imaging results.

Migration of hUC-MSCs

To better identify how stem cells repair uterine scars, we studied the fate of transplanted hUC-MSCs via *in vivo* imaging. The uteruses were significantly visualized after the injection of hUC-MSCs on the first day. Moreover, hUC-MSCs stained with GFP could be observed at days 15 and 30. However, these fluorescence signals gradually weakened in the uterus and accumulated in other organs at day 60 (Fig. 5). Consisitently, at day 60, there were no significant differences in the expression of angiogenesis-related factors.

Differential expression of microRNA and function prediction

We analyzed the global expression of microRNAs in the hUC-MSCs and PBS groups using high-throughput screening. Wide variance was seen in the abundance of different miRNAs between these two groups. MicroRNAs with higher abundance in the hUC-MSC group than in the CS group were considered hUC-MSC-specific microRNAs, and their target functions were predicted by GeneOntology (GO) analysis (Fig. 6). In KEGG analysis, we found that abundant hUC-MSC-specific microRNAs targeted cell pathways of angiogenesis and the PI3K/AKT signaling pathway. The PI3K-Akt pathway stimulates angiogenesis [28, 29].

Discussion

At present, MSC transplantation is widely used to treat diverse diseases. hUC-MSCs are favored for their source, lack of ethical complications, and noninvasive retrieval procedures [30, 31]. Taking these advantages into account, we chose to use hUC-MSCs to repair uterine scars in rats.

The repair of uterine scars involves three phases, similar to other types of wound healing: inflammation, tissue repair, and tissue remodeling [32]. We observed that hUC-MSCs secrete sufficient amounts of cytokines to promote angiogenesis and anti-scarring and improve the repair of uterine scars. FGF-2, a member of the fibroblast growth factor family, plays an important role in stimulating microvascular formation [33]. Conditioned medium derived from FGF-2-modified hUC-MSCs enhances the migration and angiogenesis of human umbilical vein endothelial cells [34]. In this study, we found that FGF-2 was significantly increased compared hUC-MSCs group with CS and PBS groups at days 15 and 30 after CS.

VEGF, the most specific pro-angiogenic factor, plays a significant role in tissue repair and regeneration [35]. VEGFA and FGF-2 are potent and well-studied factors that regulate angiogenesis, and they can promote cell proliferation and differentiation in endothelial cells [36–38]. The upregulation of VEGF expression induces the differentiation of BM-MSCs into endothelial cells [39]. Consistent with this, our data demonstrated that VEGFA was augmented in the hUC-MSC group relative to the CS and PBS groups at days 15 and 30 after CS.

PDGFB is a critical regulatory molecule in wound healing and atherosclerosis [40]. PDGF acts directly and via subsequent secretion of multiple secondary growth factors through PDGF-activated dermal fibroblasts [41]. In addition, PDGFB induces differentiation of MSCs into myofibroblasts [41]. PDGF varies consistently with FGF-2 and VEGFA at days 15 and 30 after CS. In this study, at day 60, FGF-2, VEGFA, and PDGFB showed no significant differences among the groups. This may have something to do with the survival times of stem cells.

Our *in vivo* imaging results indicated the migration of hUC-MSCs in the uteruses of dual-injured rats. It is worth noting that the number of cells gradually decreased with transplantation time, in line with the fact that MSCs remain in the body for a short time and become cleared over time [42]. MicroRNAs are among the most important types of functional molecules in MSCs. However, there is little evidence to indicate that hUC-MSCs facilitate uterine scar repair after CS through microRNAs. Our results indicate that some microRNAs have sufficient biological function to promote angiogenesis. Nevertheless, their target genes have not been identified. Although we identified some positive results in our research, many urgent questions remain. For instance, local residence time, the survival time of stem cells, and microRNAs' target genes are as yet not determined. More work is required to understand the repair functions of uterine scars.

Conclusion

hUC-MSCs have the capacity to repair, and promote the healing of uterus scars and to alleviate excessive fibrosis. Considering the significance of uterine scar healing to embryonic implantation and pregnancy, the treatment of uterine scars has important clinical significance and value.

Abbreviations

Uterine scar after cesarean section (CS)

human umbilical cord mesenchymal stem cells (hUC-MSCs)

Hematoxylin and eosin (H&E)

cesarean scar pregnancy (CSP)

Declarations

Acknowledgements

We thank Beijing Health & Biotech group for providing hUC-MSCs for us.

Authors' contributions

Xiuyin Shen: Conceptualization, investigation, methodology, and writing-original draft.

Xin Luo: Conceptualization, investigation, methodology and writing-original draft., Data curation and formal analysis. Shuzhen Wu: Resources. Yingchun Wan: Resources. Huiting Ma: Investigation. Zhuoling Zhang: Investigation. Shaoxin Ye: Resources. HaiTang: Software. Xiaoyan Gou: Software. Min Lu: editing. Xiaoling Guo: Supervision and project administration. Zhengping Liu: Supervision and project administration. The authors read and approved the final manuscript.

Funding

This work is supported by Foshan key fields of science and technology project (2020001005861). Medical Research Project of Foshan Health Bureau (20220809A010251) Project of Educational Commission of Guangdong Province (2018GkQNCX085).the Basic and Applied Basic Research Foundation of Guangdong Province (No. 2021A1515110802, G.D.C.)

Availability of data and materials

The datasets used and analyzed during our study are available from the corresponding author on reasonable request.

Ethics approval and consent to participate

All the animal experimental procedures were performed in accordance with the guidelines (PZ17010) and approved by Animal Care and Use Committee of Guangzhou University of Chinese Medicine.

Consent for publication

Not applicable.

Competing interests

The authors declare no competing interests.

References

1. Wells, J.C., R. Wibaek and M. Poullas, Global epidemiology of use of and disparities in caesarean sections. Lancet, 2019. 394(10192): p. 24-25.
2. Bergholt, T., et al., Maternal age and risk of cesarean section in women with induced labor at term-A Nordic register-based study. Acta Obstet Gynecol Scand, 2020. 99(2): p. 283-289.

3. Ioscovich, A., Y. Gozal and D. Shatalin, Anesthetic considerations for repeat cesarean section. Curr Opin Anaesthesiol, 2020. 33(3): p. 299-304.
4. Zhou, X., H. Li and X. Fu, Identifying possible risk factors for cesarean scar pregnancy based on a retrospective study of 291 cases. J Obstet Gynaecol Res, 2020. 46(2): p. 272-278.
5. Litwicka, K. and E. Greco, Caesarean scar pregnancy: a review of management options. Curr Opin Obstet Gynecol, 2013. 25(6): p. 456-61.
6. Identifying possible risk factors for cesarean scar pregnancy.
7. Hu, M.S., et al., Mesenchymal Stromal Cells and Cutaneous Wound Healing: A Comprehensive Review of the Background, Role, and Therapeutic Potential. Stem Cells Int, 2018. 2018: p. 6901983.
8. Lasocka, I., et al., The effects of graphene and mesenchymal stem cells in cutaneous wound healing and their putative action mechanism. Int J Nanomedicine, 2019. 14: p. 2281-2299.
9. Ghieh, F., et al., The Use of Stem Cells in Burn Wound Healing: A Review. Biomed Res Int, 2015. 2015: p. 684084.
10. Maranda, E.L., L. Rodriguez-Menocal and E.V. Badiavas, Role of Mesenchymal Stem Cells in Dermal Repair in Burns and Diabetic Wounds. Curr Stem Cell Res Ther, 2017. 12(1): p. 61-70.
11. Wang, X., Stem cells in tissues, organoids, and cancers. Cellular and molecular life sciences : CMLS, 2019. 76(20): p. 4043-4070.
12. Shi, X., Q. Chen and F. Wang, Mesenchymal stem cells for the treatment of ulcerative colitis: a systematic review and meta-analysis of experimental and clinical studies. Stem Cell Res Ther, 2019. 10(1): p. 266.
13. Curtis, E., et al., A First-in-Human, Phase I Study of Neural Stem Cell Transplantation for Chronic Spinal Cord Injury. Cell Stem Cell, 2018. 22(6): p. 941-950.e6.
14. Aslam, S., et al., Umbilical cord-derived mesenchymal stem cells preconditioned with isorhamnetin: potential therapy for burn wounds. World J Stem Cells, 2020. 12(12): p. 1652-1666.
15. Jeschke, M.G., et al., Allogeneic mesenchymal stem cells for treatment of severe burn injury. Stem Cell Res Ther, 2019. 10(1): p. 337.
16. Mansilla, E., et al., Cadaveric bone marrow mesenchymal stem cells: first experience treating a patient with large severe burns. Burns Trauma, 2015. 3: p. 17.
17. Abo-Elkheir, W., et al., Role of cord blood and bone marrow mesenchymal stem cells in recent deep burn: a case-control prospective study. 2017. p. 23-35.
18. Kim, S., et al., Exosomes Secreted from Induced Pluripotent Stem Cell-Derived Mesenchymal Stem Cells Accelerate Skin Cell Proliferation. Int J Mol Sci, 2018. 19(10).
19. Naji, A., et al., Biological functions of mesenchymal stem cells and clinical implications. Cell Mol Life Sci, 2019. 76(17): p. 3323-3348.
20. Zhang, L., et al., Transplantation of umbilical cord-derived mesenchymal stem cells promotes the recovery of thin endometrium in rats. Sci Rep, 2022. 12(1): p. 412.

21. Xu, Y., et al., Umbilical cord-derived mesenchymal stem cells isolated by a novel explantation technique can differentiate into functional endothelial cells and promote revascularization. Stem Cells Dev, 2010. 19(10): p. 1511-22.
22. Cao, Y., et al., Allogeneic cell therapy using umbilical cord MSCs on collagen scaffolds for patients with recurrent uterine adhesion: a phase I clinical trial. Stem Cell Res Ther, 2018. 9(1): p. 192.
23. Xin, L., et al., A collagen scaffold loaded with human umbilical cord-derived mesenchymal stem cells facilitates endometrial regeneration and restores fertility. Acta Biomater, 2019. 92: p. 160-171.
24. Zhang, L., et al., Therapeutic effect of human umbilical cord-derived mesenchymal stem cells on injured rat endometrium during its chronic phase. Stem Cell Res Ther, 2018. 9(1): p. 36.
25. Xu, L., et al., Umbilical cord-derived mesenchymal stem cells on scaffolds facilitate collagen degradation via upregulation of MMP-9 in rat uterine scars. Stem Cell Res Ther, 2017. 8(1): p. 84.
26. Fan, D., et al., Mesenchymal stem cells in the treatment of Cesarean section skin scars: study protocol for a randomized, controlled trial. Trials, 2018. 19(1): p. 155.
27. Fan, D., et al., Efficacy and safety of umbilical cord mesenchymal stem cells in treatment of cesarean section skin scars: a randomized clinical trial. Stem Cell Res Ther, 2020. 11(1): p. 244.
28. Hung, S.C., et al., Angiogenic effects of human multipotent stromal cell conditioned medium activate the PI3K-Akt pathway in hypoxic endothelial cells to inhibit apoptosis, increase survival, and stimulate angiogenesis. Stem Cells, 2007. 25(9): p. 2363-70.
29. Dai, J., et al., Osteopontin induces angiogenesis through activation of PI3K/AKT and ERK1/2 in endothelial cells. Oncogene, 2009. 28(38): p. 3412-22.
30. Todeschi, M.R., et al., Transplanted Umbilical Cord Mesenchymal Stem Cells Modify the In Vivo Microenvironment Enhancing Angiogenesis and Leading to Bone Regeneration. Stem Cells Dev, 2015. 24(13): p. 1570-81.
31. Watson, N., et al., Discarded Wharton jelly of the human umbilical cord: a viable source for mesenchymal stromal cells. Cytotherapy, 2015. 17(1): p. 18-24.
32. Wilkinson, H.N. and M.J. Hardman, Wound healing: cellular mechanisms and pathological outcomes. Open Biol, 2020. 10(9): p. 200223.
33. Wu, J., et al., Comparative Study of Heparin-Poloxamer Hydrogel Modified bFGF and aFGF for in Vivo Wound Healing Efficiency. ACS Appl Mater Interfaces, 2016. 8(29): p. 18710-21.
34. Jin, S., et al., Conditioned medium derived from FGF-2-modified GMSCs enhances migration and angiogenesis of human umbilical vein endothelial cells. Stem Cell Res Ther, 2020. 11(1): p. 68.
35. Xu, Q., W.X. Sun and Z.F. Zhang, High expression of VEGFA in MSCs promotes tendon-bone healing of rotator cuff tear via microRNA-205-5p. Eur Rev Med Pharmacol Sci, 2019. 23(10): p. 4081-4088.
36. Dworacka, M., et al., Statins in low doses reduce VEGF and bFGF serum levels in patients with type 2 diabetes mellitus. Pharmacology, 2014. 93(1-2): p. 32-8.
37. Wilcke, I., et al., VEGF(165) and bFGF protein-based therapy in a slow release system to improve angiogenesis in a bioartificial dermal substitute in vitro and in vivo. Langenbecks Arch Surg, 2007.

392(3): p. 305-14.
38. Zhu, Z., X. Gan and H. Yu, NF-κB-miR15a-bFGF/VEGFA axis contributes to the impaired angiogenic capacity of BM-MSCs in high fat diet-fed mice. Molecular medicine reports, 2017. 16(5): p. 7609-7616.
39. Sun, X., L. Luo and J. Li, LncRNA MALAT1 facilitates BM-MSCs differentiation into endothelial cells via targeting miR-206/VEGFA axis. Cell Cycle, 2020. 19(22): p. 3018-3028.
40. Ross, R., E.W. Raines and D.F. Bowen-Pope, The biology of platelet-derived growth factor. Cell, 1986. 46(2): p. 155-69.
41. Nedeau, A.E., et al., A CXCL5- and bFGF-dependent effect of PDGF-B-activated fibroblasts in promoting trafficking and differentiation of bone marrow-derived mesenchymal stem cells. Exp Cell Res, 2008. 314(11-12): p. 2176-86.
42. Yang, Z., et al., Options for tracking GFP-Labeled transplanted myoblasts using in vivo fluorescence imaging: implications for tracking stem cell fate. BMC Biotechnol, 2014. 14: p. 55.

Figures

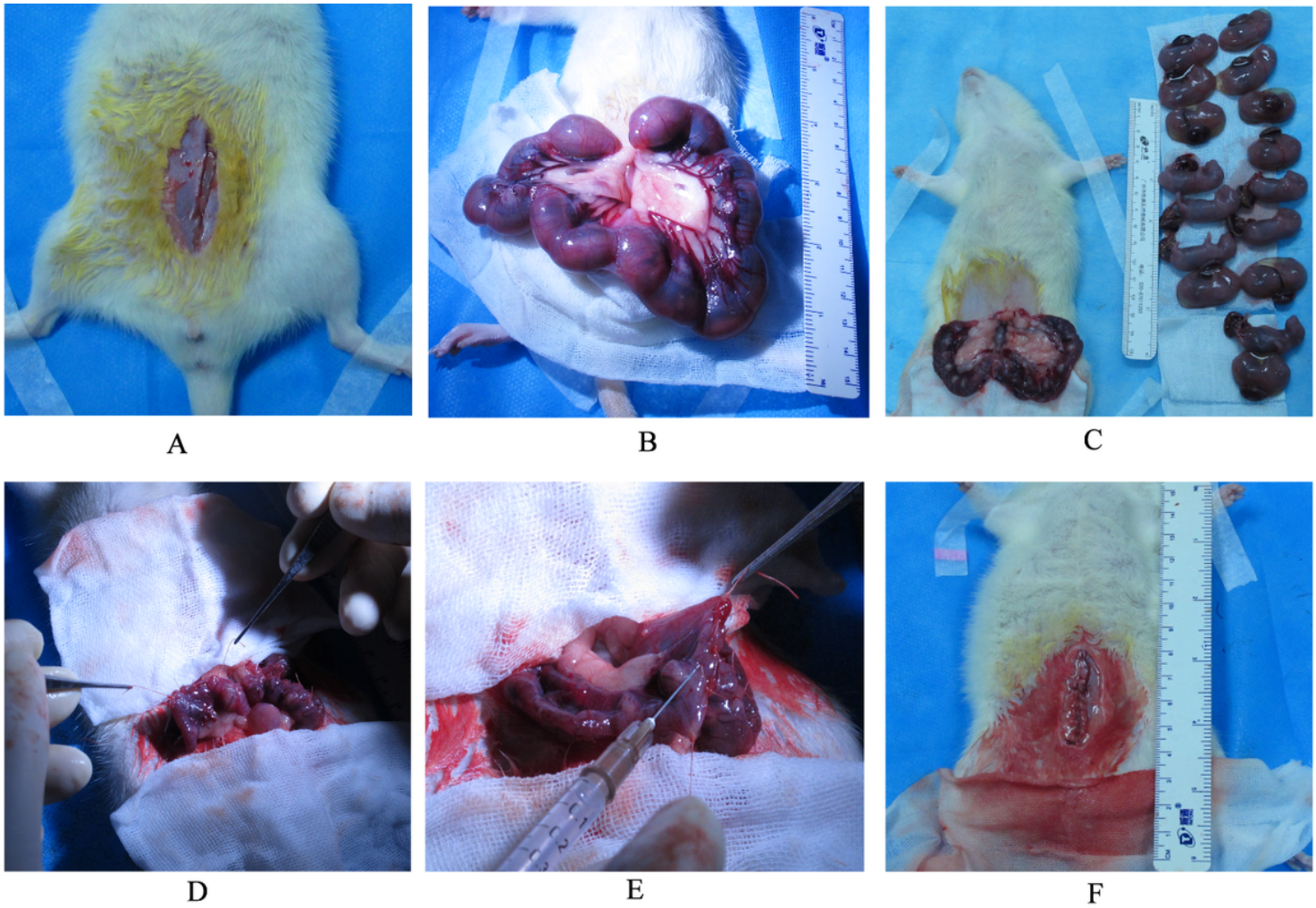

Figure 1

Establishment and treatments of a rat model of uterine scars. After the rats were anesthetized by intraperitoneal injection of 10% chloral hydrate (35 mg/kg), a low abdominal midline incision was made to expose the uterine horns and to take out and remove the fetuses (A–C). The uterine incisions were sutured continuously with 4-0 absorbable Vicchio (D). PBS and hUC-MSCs were injected per uterine horn in PBS and hUC-MSC groups (E). After rinsing the abdominal cavity with saline, the skin was sutured with a 4-0 silk suture in an uninterrupted fashion (F).

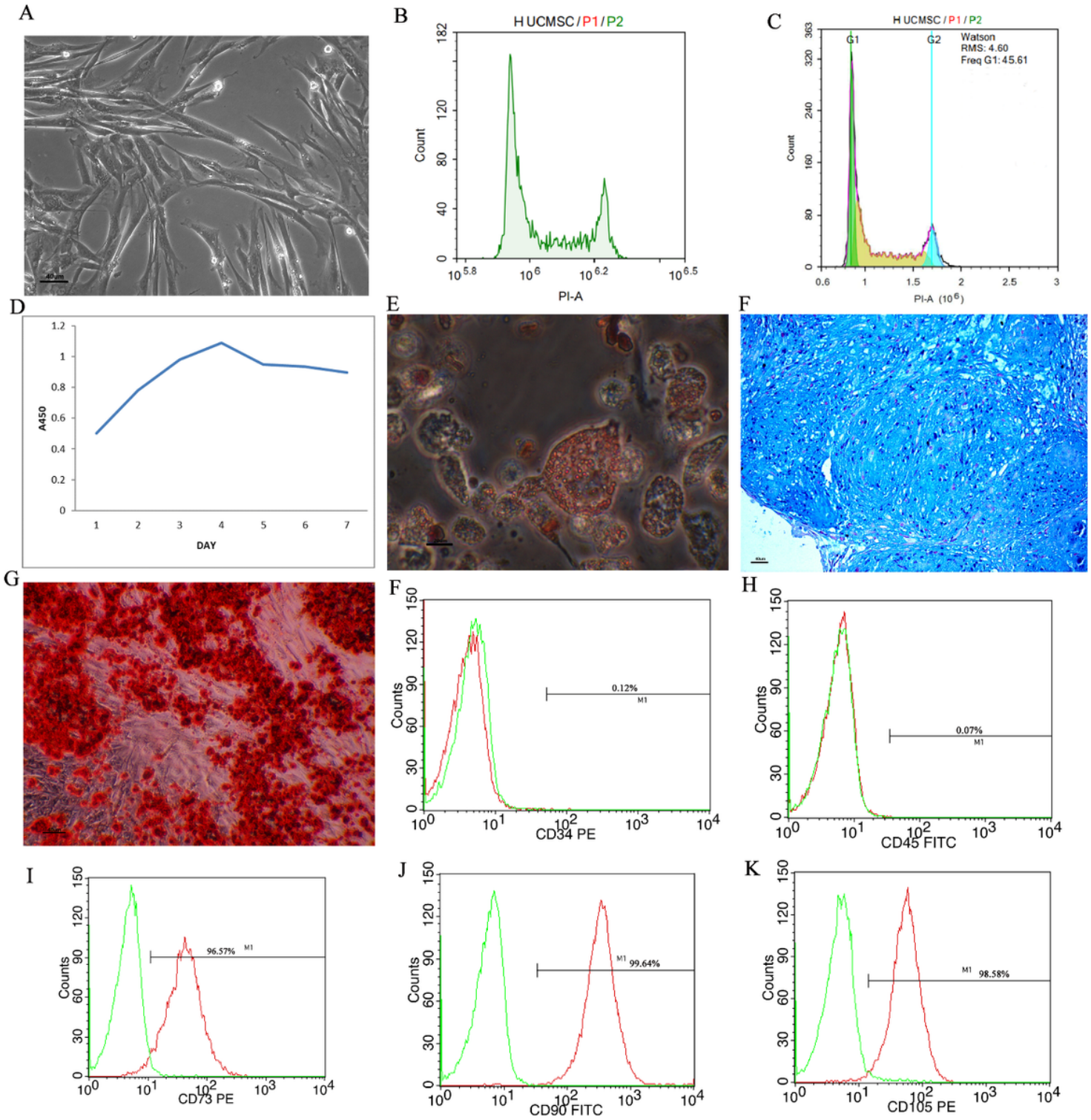

Figure 2

hUC-MSC culture and identification. The hUC-MSCs maintained a mesenchymal-like morphology (A). Distribution of cell cycle (B). The cells at passage 3 exhibited a good proliferation rate (C). After 14 days of adipogenic induction, the cells formed lipid droplets stained by oil red O (D). After 21 days of chondroblastic induction, the cells formed acidic mucopolysaccharide stained with alcian blue (E). After 21 days of osteogenic induction, the cells formed mineralized nodules stained with alizarin red (F). In flow cytometric analysis, hUC-MSCs positively expressed stem cell surface markers CD73 (96.57%), CD90 (99.64%), and CD105 (98.58%) but negatively expressed CD34 (0.12%) and CD45 (0.07%) (J, K).

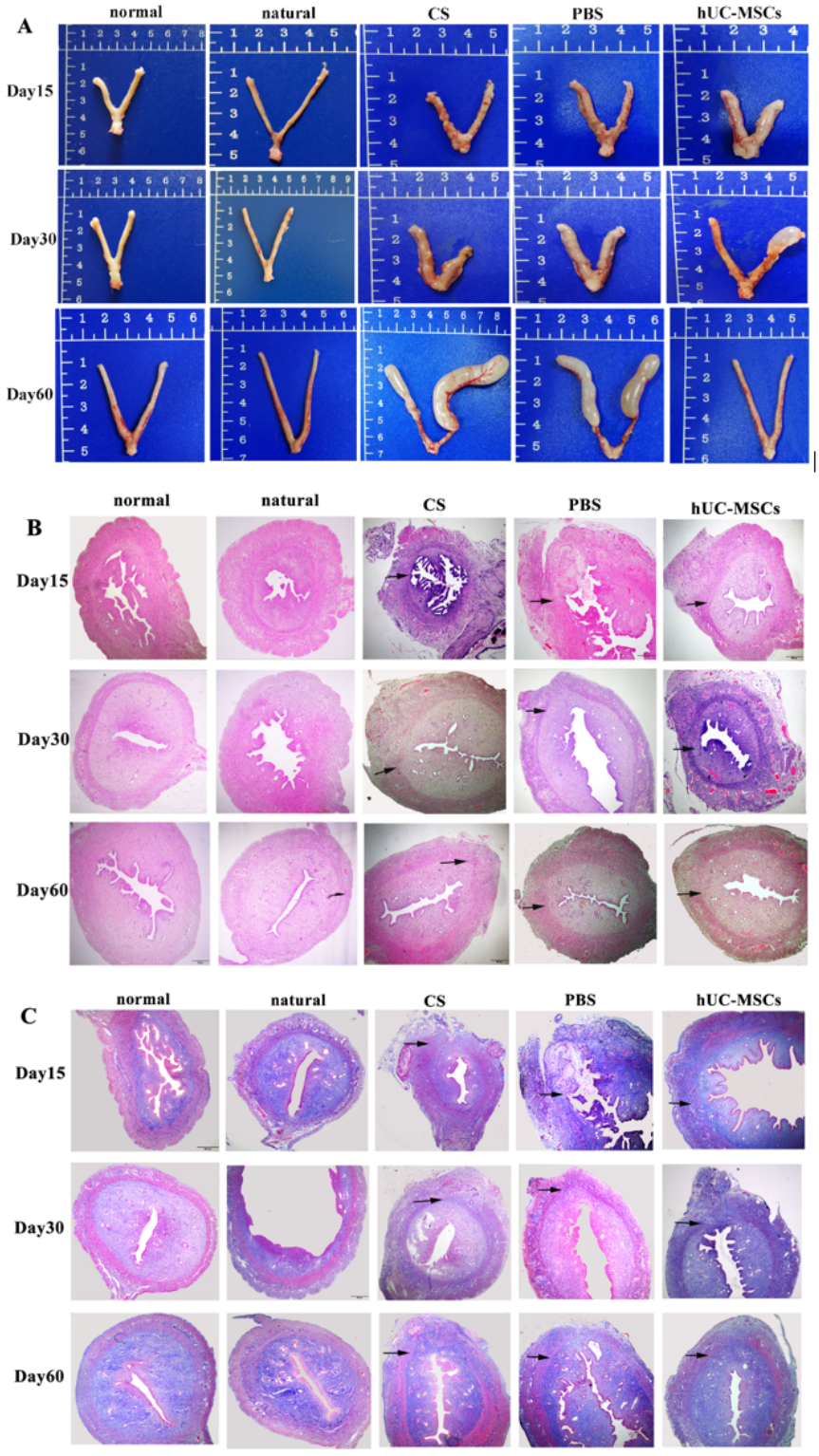

Figure 3

Uterine morphological features. The macroscopic appearance of the uterus at days 15, 30, and 60 after CS (A). H&E staining at days 15, 30, and 60 (50×) (B). Masson's trichrome staining at days 15, 30, and 60 (50×) (C).

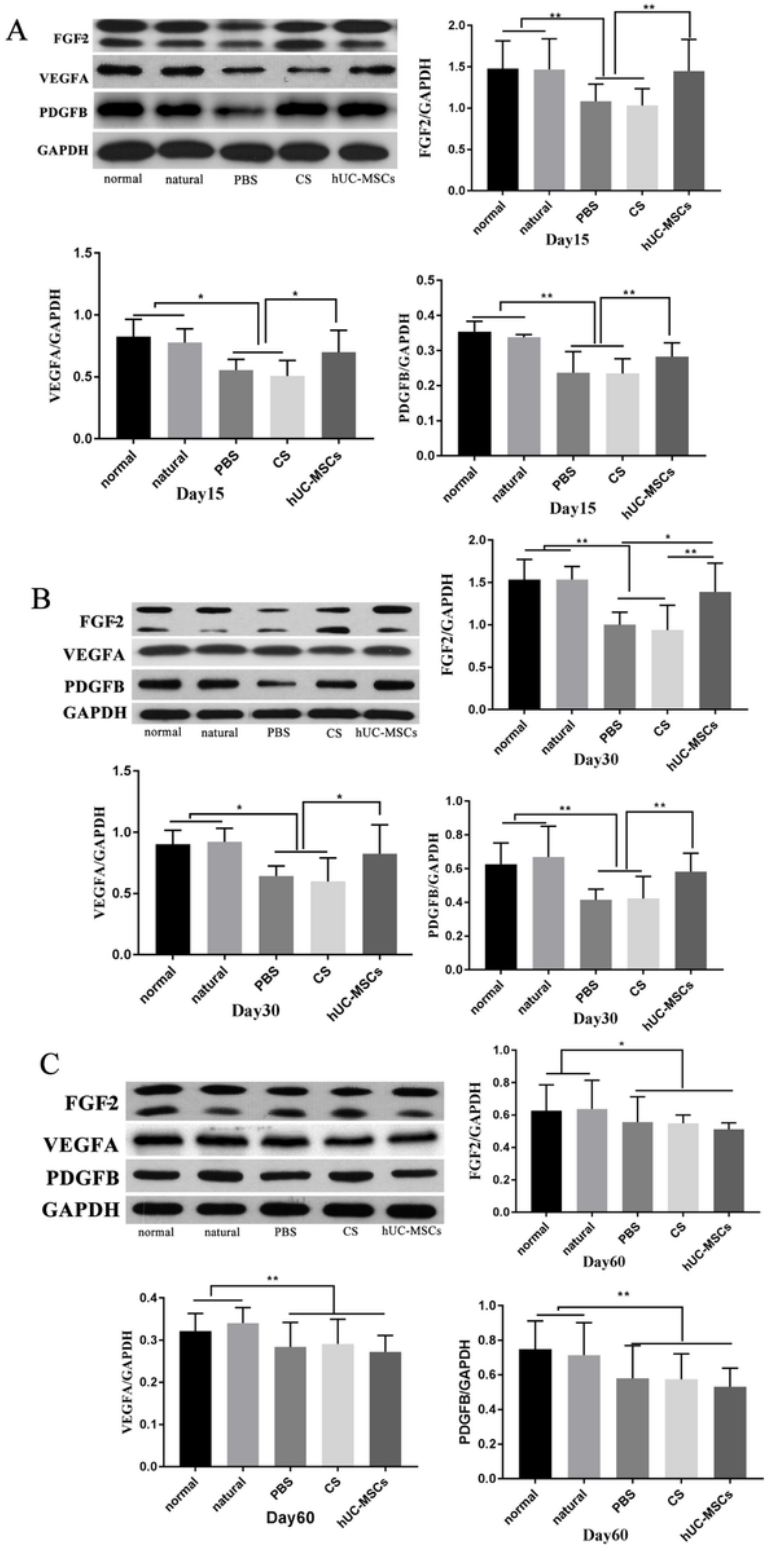

Figure 4

Effect of hUC-MSCs on angiogenesis-related factors. The expressions of FGF-2, VEGFA, and PDGFB at days 15, 30, and 60 after CS were examined by western blotting. *p < 0.05, **p < 0.01.

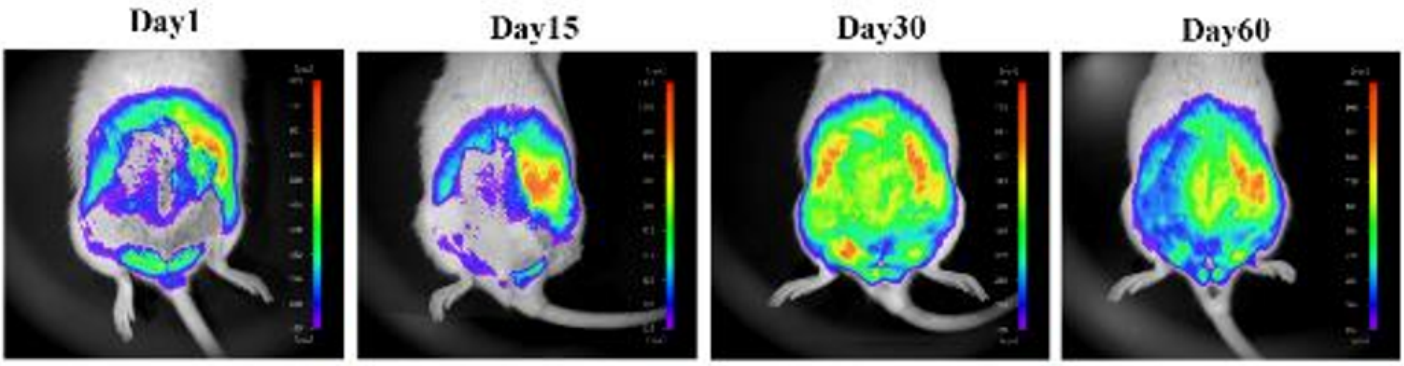

Figure 5

Results of *in vivo* imaging of hUC-MSCs stained with GFP at days 1, 15, 30, and 60.

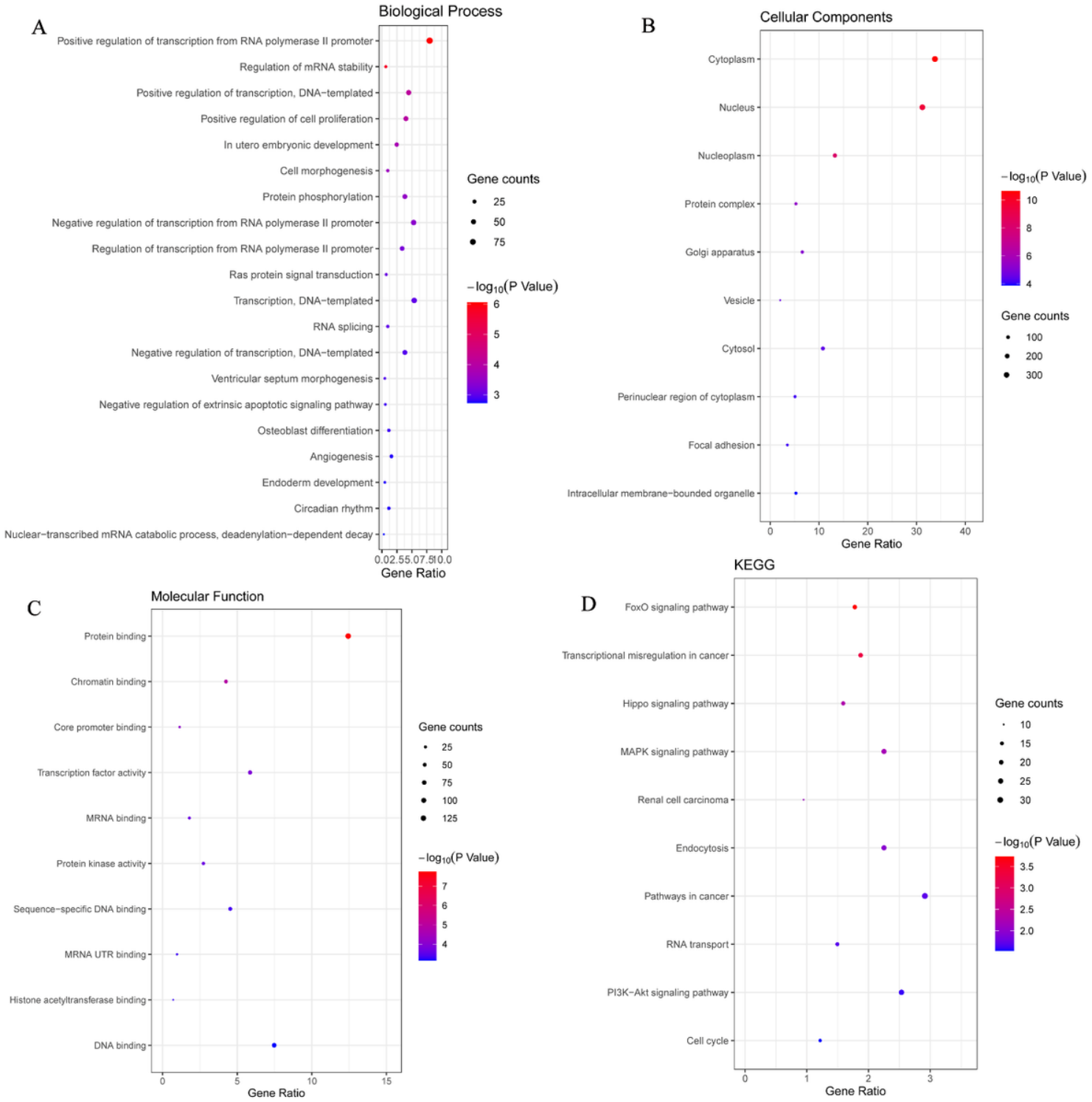

Figure 6

Differential expression of microRNA and function prediction. The biological functions of the 20 most abundant differential miRNAs (A). Results of GeneOntology analysis of the 10 most abundantly expressed differential miRNAs (B, C). Results of KEGG analysis of abundant hUC-MSC-specific microRNA-targeted pathways (D).

Supplementary Files

This is a list of supplementary files associated with this preprint. Click to download.

- supplementarymaterial.docx